Electronic Supplementary Material (ESI) for Nanoscale.

Supporting Information

Rational inert-basal-plane activating design of ultrathin 1T′ phase MoS_2 with MoO_3 heterstructure for enhancing hydrogen evolution performances

Xiaoyi Xue,[a] Jianan Zhang,[a,c] Ibrahim Saana Amiinu,[b] Jian Sun,[a] Qun Xu,*[a] and Shichun Mu,*[b]*

[a]College of Materials Science and Engineering, Zhengzhou University, Zhengzhou 450001, P. R. China. Emails: zjn@zzu.edu.cn (J. N. Zhang) and qunxu@zzu.edu.cn (Q. Xu)

[b]State Key Laboratory of Advanced Technology for Materials Synthesis and Processing, Wuhan University of Technology, Wuhan 430070, P. R. China, E-mail: msc@whut.edu.cn

[c]Key Laboratory of Advanced Energy Materials Chemistry (Ministry of Education), Nankai University, Tianjin 30071, P. R. China

1. Theoretical calculation

Details of calculations: Density Functional Theory (DFT) computations were conducted using the Cambridge Sequential Total Energy Package (CASTEP) based on the plane wave pseudopotential method.[1] The geometrical structure of the (110) plane of 1T-MoS_2 and the (100) plane of MoO_3 were optimized using the generalized gradient approximation (GGA) methods. The Revised Perdew-Burke-Ernzerhof (RPBE) functional was used to treat the electron exchange correlation (EEC) interactions. The Brillouin zone was sampled using a Monkhorst Pack k-point grid of 3×3×1 and a plane-wave basis set cut-off energy of 400 eV was applied. The cell structures were optimized for energy and force convergence threshold set at 30 meV/Å and 1.0×10^{-2} meV, respectively. A self-consistence field of 2.0×10^{-6} eV/atom and a vacuum space as large as 15.0 Å were applied to avoid periodic interactions. The ultra-soft pseudopotentials were applied for the valence electrons and ionic core interactions. To mimic the bulk properties, the top surface atomic layers were fully relaxed while the under layers remained constrained.

The Gibbs free energy (ΔG_{H*}) of chemisorbed hydrogen was calculated as the energy difference between the reactant and reaction product, that is hydrogen-adsorbed on the catalyst system and the free-state catalyst and hydrogen. The final free energy was computed as:

$$\Delta G_{H*} = E_{total} + E_{surf} - \tfrac{1}{2}E_{H2} + \Delta ZPE - T\Delta S$$

where the given symbols represent total energy (E_{total}) for adsorbed system, energy of the pure system (E_{surf}), change in zero-point-energy (ΔE_{ZPE}), the temperature of the system (T), and entropy change (ΔS), respectively. Herein, the vibrational entropy of hydrogen in the adsorbed state is approximated to be negligible such that $\Delta S_H \approx S_{H*} - \tfrac{1}{2}S_{(H2)} \approx -\tfrac{1}{2}S_{(H2}$, where $-\tfrac{1}{2}S_{(H2}$ represents the entropy of hydrogen in the gas phase at standard conditions. The standard $TS_{(H2)}$ is given to be ~0.41 eV for H_2 at 1 atm and 300 K. [2,3]

Theoretical models: The correlative models for the catalyst samples were built to simulate 1T-MoS_2, MoO_3 and their heterostructure as shown in Figure S1-3. Typically, the (100) facet of 1T-MoS_2 was modeled by the slab with layers of Mo-S bonded atoms while the (011) facet was adopted to generate the MoO_3 slab. To create the heterojunction model catalyst, the MoO_3 was laid on the 1T-MoS_2 surface and optimized, and to avoid the effect of lattice mismatch, an interface periodicity of 3×2 supercell for 1T-MoS_2 phase and 2×2 supercell for the MoO_3 phase were applied for creating the simulation model of the heterostructure. The lattice parameters for all model structures are given in Table S2. The optimized structure of 1T-MoS_2@MoO_x displays a slight distortion of the 1T-phase of MoS_2 facet after integrating the MoO_3 layer, resulting in a quasi-1T-MoS_2 phase in the heterostructure (1T′-MoS_2/MoO_x).

2. Supplementary Figures and Tables

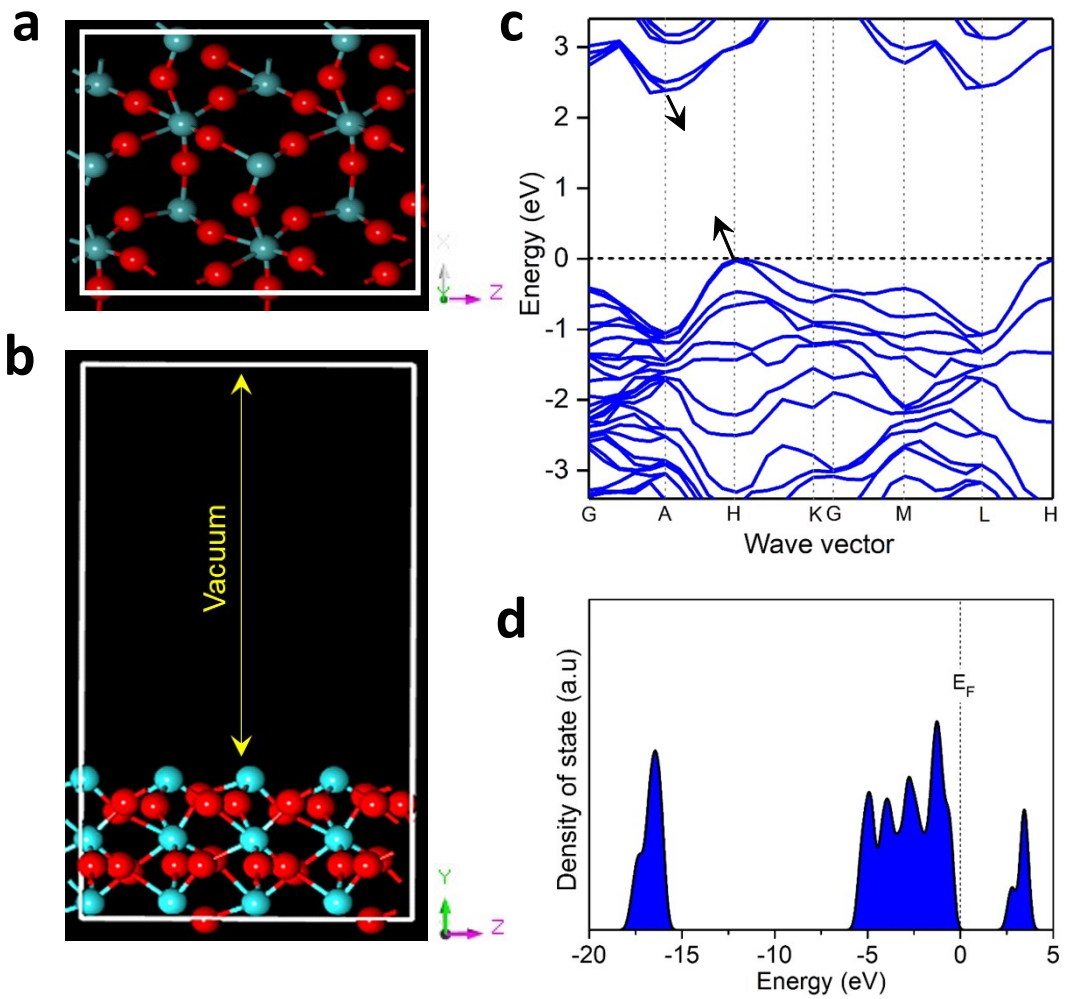

Figure S1. Structural model (a) top view and (d) side view, (c) band structure, E_g ~2.36 eV, and (d) density of state of MoO_3. Atoms are O (red) and Mo (aqua).

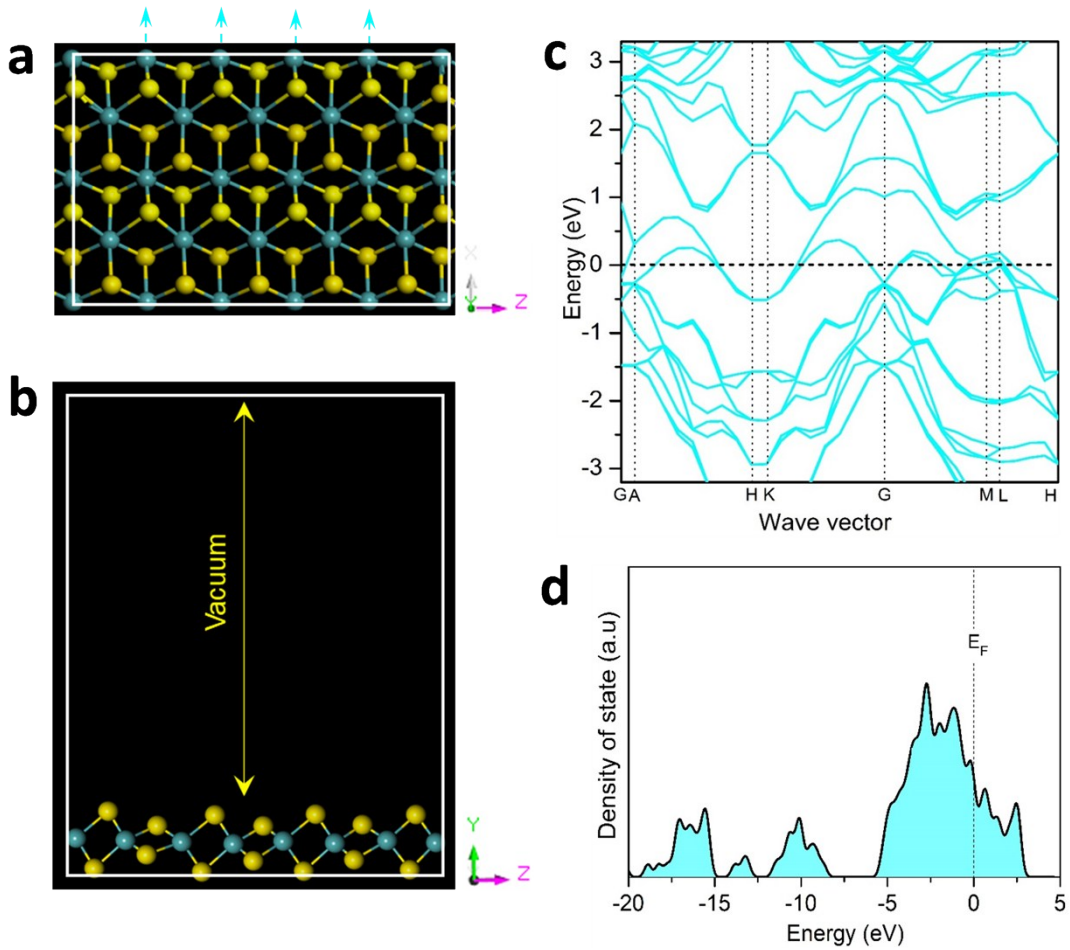

Figure S2. Structural model (a) top view and (d) side view, (c) band structure, E_g = 0.00 eV, and (d) density of state of 1T-MoS_2. Atoms are S (yellow) and Mo (aqua).

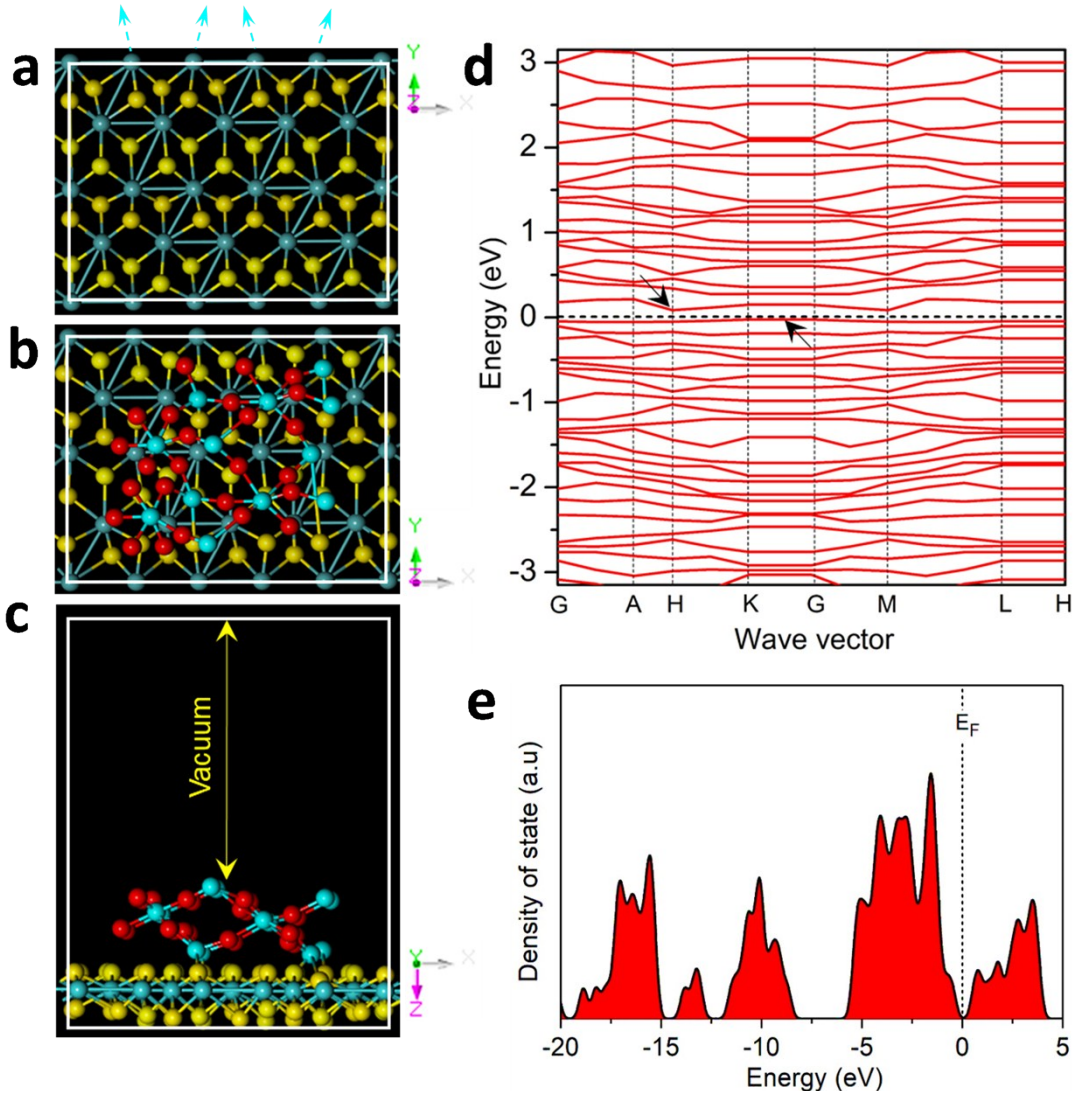

Figure S3. Structural model (a) top view of 1T′-MoS_2 and (b, c) top and side views of 1T′-MoS_2/MoO_x. (c) The band structure and (d) density of state of 1T′-MoS_2/MoO_x. Atoms are O (red), Mo (aqua), and S (yellow).

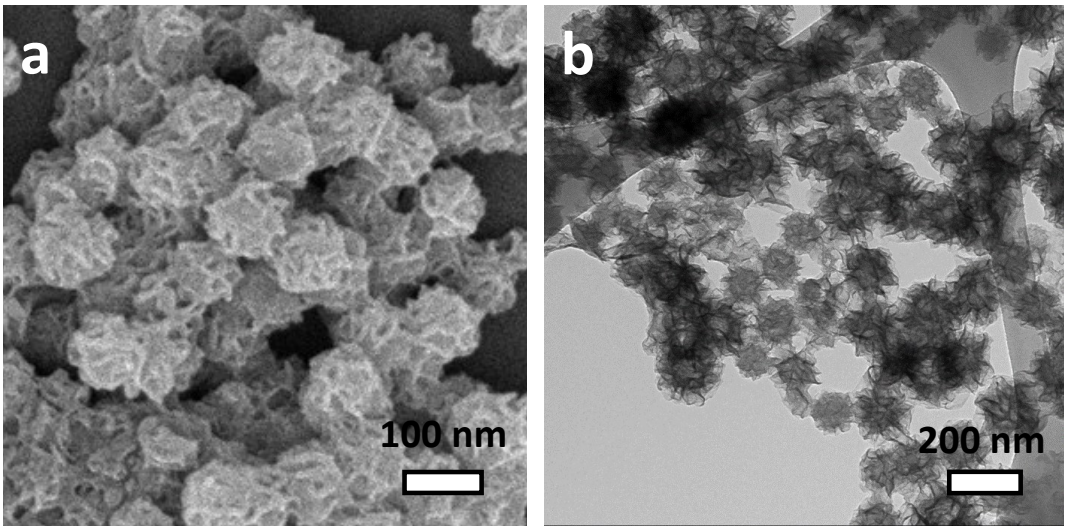

Figure S4. (a) SEM and (b) TEM images of HMHSs.

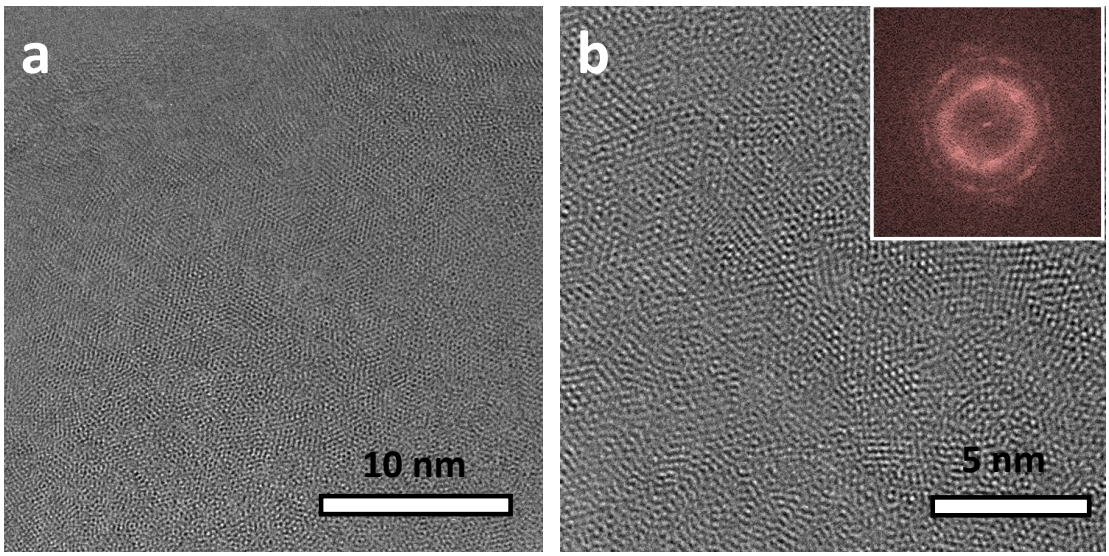

Figure S5. HRTEM images of HMHSs.

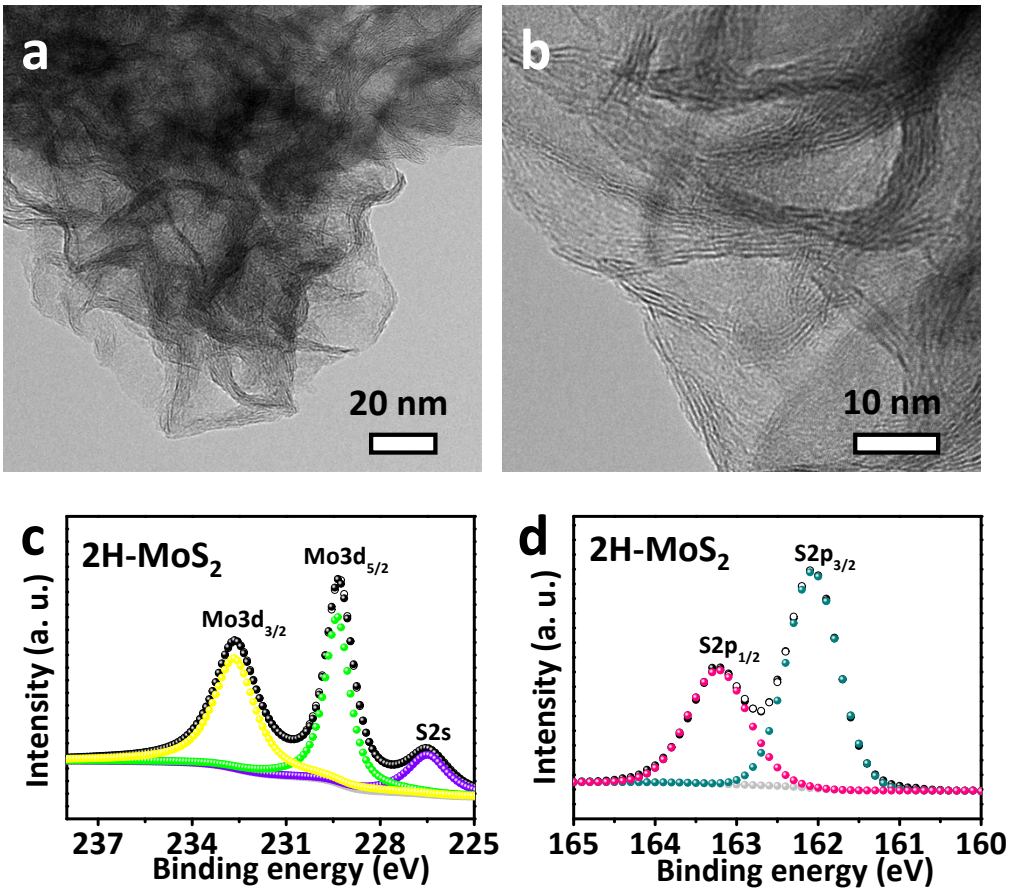

Figure S6. (a, b) TEM images of 2H-MoS_2, (c, d) high-resolution XPS spectra of Mo 3d, S 2p.

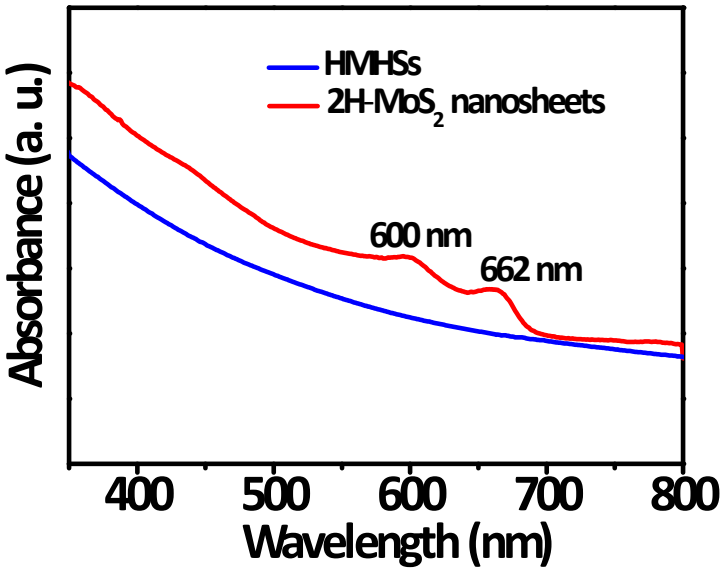

Figure S7. UV absorption spectra of HMHSs and 2H MoS_2 nanosheets.

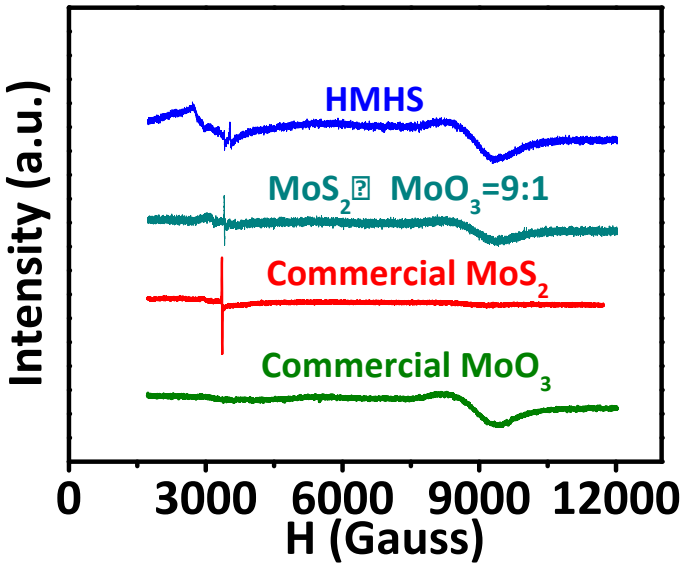

Figure S8. (a) EPR spectrum of HMHS, commercial MoS_2, commercial MoO_3, MoS_2 and MoO_3 mixture.

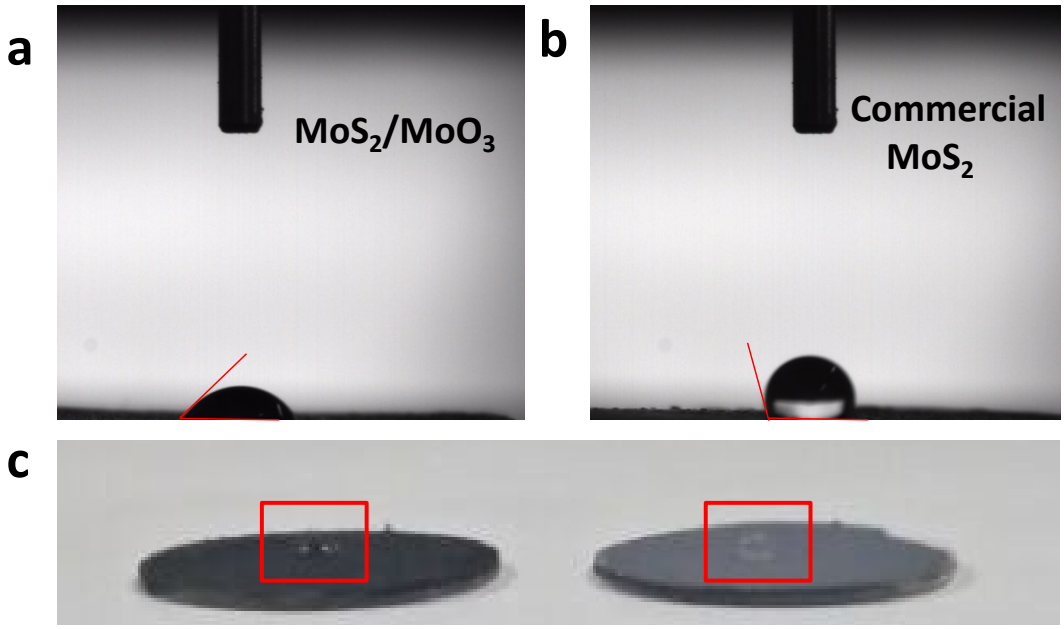

Figure S9. Static contact angle images. (a) Fresh HMHSs film. We measured the contact angle by drop casting a droplet of water (5 μL) on the HMHSs film and obtained an angle of 45°. (b) Commercial MoS_2 film. The same experiments were done on the commercial MoS_2 films and an angle of 110° was found. These results confirm the hydrophilic surface of HMHSs and hydrophobic surface of commercial MoS_2 . (c) Optical images of the HMHSs and commercial MoS_2 on Glass pieces

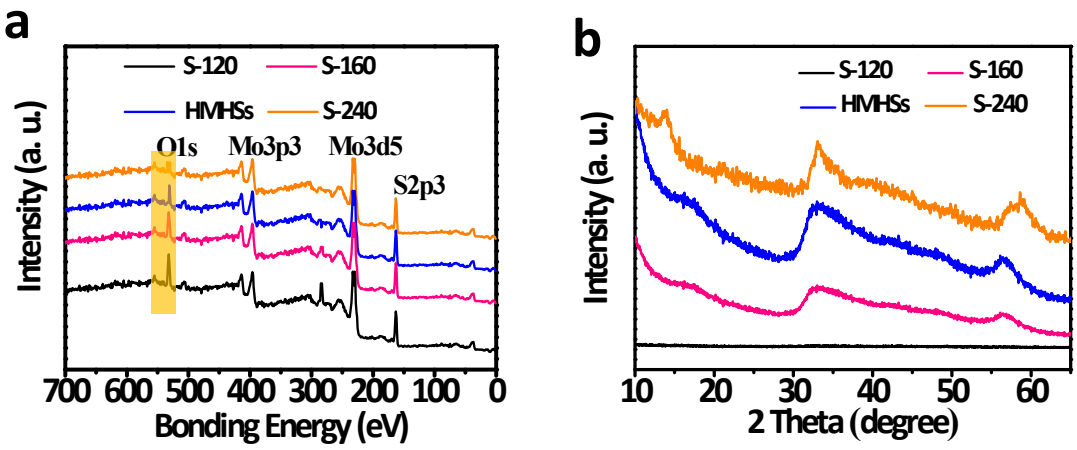

Figure S10. (a) XPS spectra and (b) XRD patterns of the S-120, S-160, HMHSs and S-240.

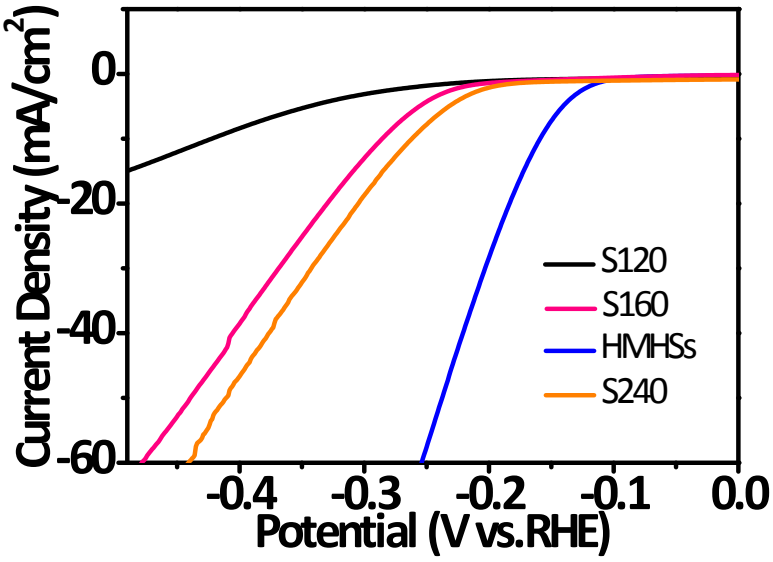

Figure S11. Polarization curves of Samples at different temperatures.

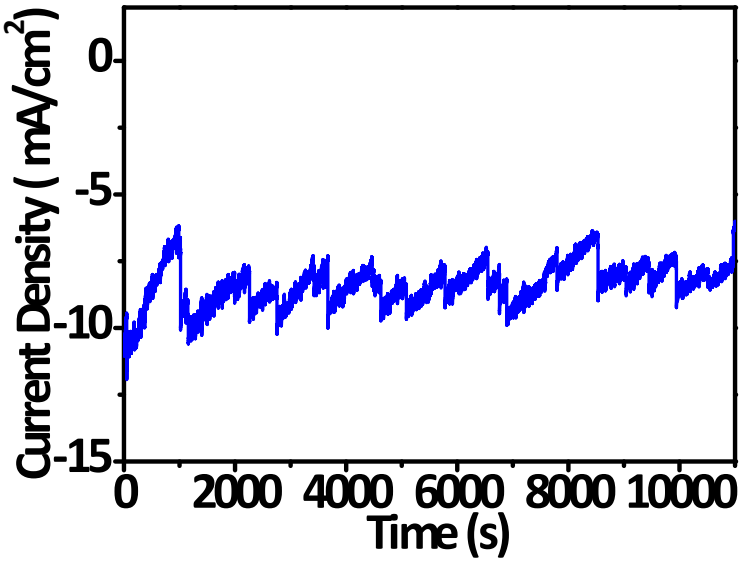

Figure S12. Time dependence of current density under static overpotential of 120 mV.

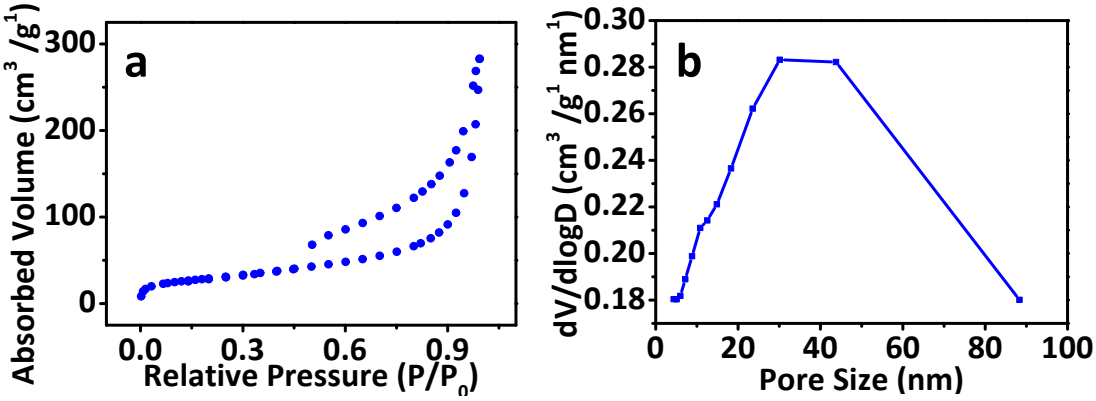

Figure S13. (a) BET nitrogen adsorption and desorption isotherms and (b) pore size distribution of the HMHSs.

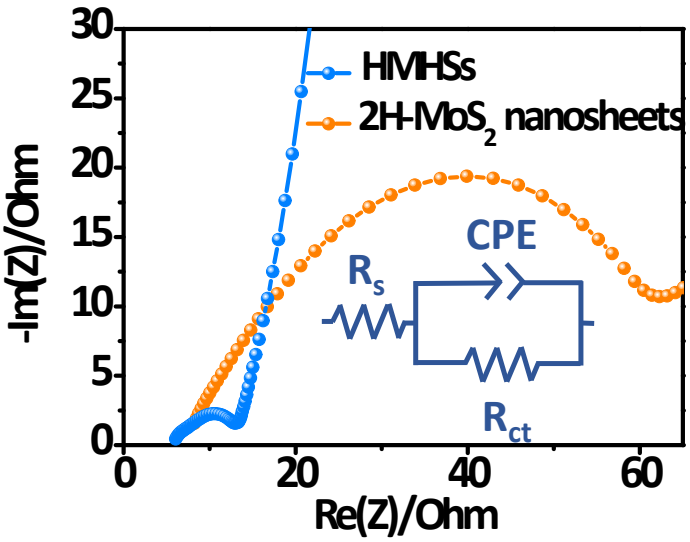

Figure S14. Nyquist plots of electrochemical impedance spectra (EIS) of HMHSs and 2H-MoS_2 nanosheets. The *inset* is the equivalent electrical circuit.

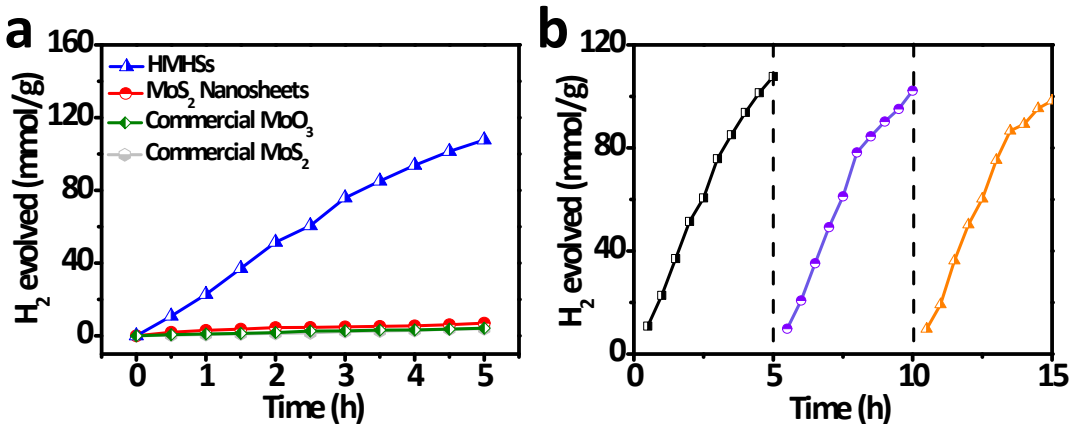

Figure S15. (a) Photocatalytic H_2 evolved of HMHS, MoS_2 nanosheets, commercial MoS_2 and MoO_3. (b) Time course of H_2 evolved of HMHSs.

In photocatalytic hydrogen production test, the mixture of eosin, triethanolamine,and deionized water was applied as the reaction medium with 300 W xenon lamp as a light source. **Figure S15a** demonstrates the HMHSs evolved the highest H_2 production of 22.108 mmol g^{-1} h^{-1}. For comparison, we also tested the hydrogen production properties of commercial MoS_2, MoS_2 nanosheets and MoO_3 nanosheets, HMHSs is 20 times higher than MoS_2 nanosheets, 27 times higher than commercial MoS_2 and 28 times higher than MoO_3 nanosheets. The stability test (**Figure S15b**) showed that the reduction in photocatalytic performance was negligible after 15 h of the reaction,suggesting its good durability. We hypothesize that good performance is due to the fact that nanospheres favors exposure to more active sites and the synergistic effect of molybdenum sulfide and molybdenum oxide. A more detailed explanation is as follows: While the metallic charater of 1T-MoS_2 may be good for enhancing electrical conductivity, it is unfavourable for the separation of photogenerated charge cariers. Similarly, the wide E_g of MoO_3 is unsuitable for enhancing electrocatalytic or photocatalytic properties due to it poor conductivity of ionic species. Interestingly, by coupling MoO_3 with 1T-MoS_2, utilizes the best properties of each component while mitigating their deficiencies, and thus realizes an effective enhancement of visible-light-driven H_2 evolution activity. What more,

the fascinating hollow structure of HMHSs provides a high BET surface area, which facilitates the exposure of more active sites to promote catalytic performance. To compare the catalytic activity of the HMHSs with those of the recently reported for Molybdenum sulfide-based catalytic, the hydrogen production rate and TOF are summarized in **Table S7**, which show our catalytic have a better catalytic capacity.

Table S1 The ΔG (H*) values of the H* adsorbed on the surface of different models.

Models	HMHSs	MoO_3	1T-MoS_2	bulk MoS_2
ΔG(H*)	~0.126 eV	~0.488 eV	~0.283 eV	~0.34 eV

Table S2 Lattice parameters (Å) of supercells for all model systems.

Model catalyst	**a**	**b**	**c**
MoO_3	10.800	9.470	20.097
1T-MoS_2	15.815	11.245	23.477
1T′-MoS_2/MoO_x	16.001	11.245	28.124

Table S3. Catalytic activity comparison samples with respect to 1T′-MoS_2/MoO_3 with different mass ratios.

Sample	**Mo**	**S**	**O**	**Mass content of MoS_2 (%)**	**η at 5 mA/cm² (V)**
S-120	10.25	7.37	18.89	22.4	0.341
S-160	10.12	10.88	14.04	37	0.253
HMHSs	9.89	13.56	9.33	54	0.092
S-240	9.77	18.24	1.23	98	0.232

Table S4. Catalytic activity comparison of these nanoframes and the reported nanocatalysts.

Catalyst	Catalyst loading (mg cm^{-2})	Tafel slope (mV dec^{-1})	Current density (j, mA cm^{-2})	η at the correspondi ng j (mV)	Ref.
HMHSs	**0.2**	**42**	**10**	**~109**	**In this work**
Ultrathin MoS_2 Nanoplates	0.136	53	10	~155	*ACS Appl. Mater. Interfaces 2013, 5, 12794*
MoS_2 nanosheets	0.0002	60	10	~250	*Nat. Mater. 2013, 12, 850*
Oxygen incorporated MoS_2	0.285	55	10	~180	*J. Am. Chem. Soc. 2013, 135, 17881*
MoS_2 nanosheets	0.05	40	10	~200	*Nano Lett. 2013, 13, 6222*
MoS_2 nanofilm	0.12	51	10	~235	*Adv. Mater. 2014, 26, 2683*
MoO_2-supported MoS_2 nanosheets	0.22	76.1	10	~220	*Nanoscale, 2015, 7, 5203*
column-like MoS_2 nanosheets	0.40	39	10	~200	*Chem. Mater. 2016, 28, 2074*
GCNF@MoS_2	0.2	49.6	10	~200	*Electrochim. Acta, 2016, 219, 604*
Pt-MoS_2	0.201	96	10	~210	*Energy Environ. Sci., 2015, 8, 1594*
MoO_3-MoS_2 Nanowires	0.2	55	10	~310	*Nano Lett. 2011, 11, 4168*
graphene/MoS_2	Ca. 1.86	47	50	~200	*RSC Adv., 2016, 6, 31359*

Table S5. Catalytic durability comparison of these nanoframes and the reported nanocatalysts.

Catalyst	Cycle number	η_{10}(mV)	IT test time (s)	IT test result	Ref.
HMHSs	**3000**	negligible decay	**10000**	**Current density reduced by 8.6%**	**In this work**
Ultrathin MoS_2 Nanoplates	2000	negligible decay	-	-	*ACS Appl. Mater. Interfaces 2013, 5, 12794*
WS_2 nanosheets	10000	remain stable	-	-	*Nat. Mater. 2013, 12, 850*
Oxygen incorporated MoS_2	3000	negligible difference	20000	slight degradation	*J. Am. Chem. Soc. 2013, 135, 17881*
MoS_2 nanosheets	-	-	-	-	*Nano Lett. 2013, 13, 6222*
MoS_2 nanofilm	1000	remain stable	21000	stable high current density	*Adv. Mater. 2014, 26, 2683*
MoO_2-supported MoS_2 nanosheets	1000	remained almost unchanged	36000	reduction currents remained almost invariant	*Nanoscale, 2015, 7, 5203*
column-like MoS_2 nanosheets	1000	few changes	-	-	*Chem. Mater. 2016, 28, 2074*
GCNF@ MoS_2	-	-	36000	Current density reduced by 18.7%	*Electrochim. Acta, 2016, 219, 604*
Pt-MoS_2	5000	a very stable performanc e	-	-	*Energy Environ. Sci., 2015, 8, 1594*
MoO_3-MoS_2 Nanowires	10000	No degradation	-	-	*Nano Lett. 2011, 11, 4168*
graphene/MoS_2	1000	little current lost	3000	reduction currents remained almost invariant	*RSC Adv., 2016, 6, 31359*

Table S6. Catalytic activity comparison of the HMHSs, molybdenum compounds and other non-precious metal catalysts.

Catalyst	Catalyst loading (mg cm^{-2})	Tafel slope (mV dec^{-1})	Current density (j, mA cm^{-2})	η at the correspondi ng j (mV)	Ref.
HMHSs	**0.2**	**42**	**10**	**~109**	**In this work**
①MoS_2 nanomesh	0.28	46	10	~160	*10.1016/j.apcatb.20 18.05.080*
②NiCoMo film	-	65.3	10	~35	*ACS Appl. Mater. Interfaces, 2017, 9, 22420*
③$MoSe_2$/ MoO_2/Mo	-	48.9	10	~142	*Small 2018, 14, 1703798*
④MoP/CNT-700	0.5	60	10	~83	*Adv. Funct. Mater. 2018, 28, 1706523*
⑤NC-$Co_{0.85}Se$	0.57	34.1	30	~210	*Electrochim. Acta, 2017, 247, 468*
⑥WxC/NG-10	0.5659	45.91	10	~77.82	*Electrochim. Acta, 2017, 251, 660*
⑦C-WP/W	-	79.8	10	~109	*Chem. Eng. J., 2017, 327, 705*
⑧GNS	0.28	35.8	25	~ 290	*Electrochim. Acta, 2018, 283, 1146e1153*
⑨Petaloid FeP/C	0.28	57	10	~ 110	*Electrochem. Commun., 2018, 92, 33*
⑩ZnSe/$MoSe_2$	0.75	73	10	~ 200	*Adv. Mater. Interfaces, 2017, 1700948*

Table S7. Activity of catalyst in terms of yield of H_2 evolved and TOF.

Photocatalyst	Light source	Activity[mmolg^{-1}h^{-1}]	TOF[a][h^{-1}]	Ref.
HMHS	300 W Xe lamp	22	5.25	In this work
Colloidal MoS_2	300 W Xe lamp	-	6	*Chem. Commun. 2009, 0, 4536.*
MoS_2/CdS	300 W Xe lamp	5.3	ca. 0.7	*J. Am. Chem. Soc. 2008, 130, 7176*
CdSe-MoS_2	300 W Xe lamp	0.8	ca. 0.15	*J. Phys. Chem. C 2010, 114, 10628*
MoS_2/SiO_2	Hg Lamp	0.86	ca. 0.14	*J. Catal. 1991, 131, 156*
MoS_2/TiO_2	300 W Xe lamp	0.03	ca. 0.005	*J. Colloid Interface Sc. 2011, 354, 607*
TiO_2/MoS_2/graphene	300 W Xe lamp	2.1	ca. 0.35	*J. Am. Chem. Soc. 2012, 134, 6575*
MoS_xC_y	300 W Xe lamp	19	ca. 0.3	*Dalton Trans. 2013,42, 1287*
MoS_2/RGO	300 W Xe lamp	4.19	1.00	*J. Phys. Chem. C 2012, 116, 25415*
p-MoS_2/n-RGO	300 W Xe lamp	0.025	0.006	*J. Am. Chem. Soc. 2013, 135, 10286*
MoS_2/TiO_2	300 W Xe lamp	0.75	0.18	*Phys. Chem. Chem. Phys. 2015, 17, 933*
TiO_2/MoS_2/G	350 W Xe lamp	2.07	0.49	*J. Am. Chem. Soc., 2012, 134 (15), pp 6575*
TiO_2@MoS_2	300 W Xe lamp	1.68	0.40	*Appl. Catal. B 2015, 164, 1*
1T MoS_2	100 W halogen	26	6.2	*Angew. Chem. Int. Ed. 2013, 52, 13057*
MoS_2-NH_3	150 W halogen	0.171	0.04	*J. Alloy Compd. 2016, 688, 368*

References

1. M. Segall, P. J. Lindan, M. Probert, C. Pickard, P. Hasnip, S. Clark and M. Payne, *J. Phys. Condens. Matter,* 2002, **14**, 2717-2744.

2. J. K. Nørskov, T. Bligaard, A. Logadottir, J. R. Kitchin, J. G. Chen, S. Pandelov and U. Stimming, *J. Electrochem. Soc.,* 2005, **152**, J23-J26.

3. Y. Liu, G. Yu, G. D. Li, Y. Sun, T. Asefa, W. Chen and X. Zou, *Angew. Chem. Int. Ed.,* 2015, **54**, 10752-10757.